Department of Physics and Astronomy
University of Heidelberg

Bachelor Thesis in Physics
submitted by

Nils Heyer

born in Gießen (Germany)

July 2019

Performance Test of a 20 Gap Resistive Plate Chamber Prototype Built with Thin Low Resistive Float Glass

This Bachelor Thesis was carried out by Nils Heyer at the Physikalisches Institut at the University of Heidelberg under the supervision of Prof. Dr. Norbert Herrmann

Abstract

At the March 2019 beamtime of the mCBM experiment a 20 gap multi strip resistive plate chamber built with low resistive float glass was introduced to the mTOF setup to evaluate the performance of the new low resistive glass for future detectors. In order to analyze the performance of the prototype, the efficiency was approximated for different high voltages to find the working voltage. Because the results of the evaluation did not reflect an efficiency well above the expected 95%, the rate dependency of the efficiency was analyzed. This evaluation suggests data loss in the read out chain. Further indications of this conclusion occurred after comparison of the detector rates versus the currents in the detector. The highest efficiency measured at mCBM was 59.1% with a time resolution of 102.7ps.

Abstract

Während der im März 2019 stattfindenden Strahlzeit des mCBM Experiments wurde ein 20 Spalten MRPC, welcher mit niederohmigem Glas gebaut wurde, in den mTOF Aufbau integriert, um die Performance des neuen niederohmigen Glases für zukünftige Detektoren zu evaluieren. Die Analyse des Prototyps beinhaltete eine Effizienzapproximation für verschiedene Hochspannungseinstellungen, um die Arbeitsspannung zu finden. Da die Resultate nicht wie erwartet Effizienzen im Bereich von über 95% lieferten, wurde die Ratenabhängigkeit der Effizienz untersucht, welche auf einen Datenverlust in der Ausleseelektronik hindeuten würde. Um den Datenverlust weiter zu untersuchen wurden die vom Detektor gemessenen Raten mit den im Detektor gemessenen Strömen verglichen. Die höchste Effizienz, welche im mCBM Experiment gemessen wurde, lag bei 59.1% mit einer Zeitauflösung von 102.7ps.

Contents

1 Introduction

The Compressed Baryonic Matter experiment (CBM), considered to be built at the "Gesellschaft für Schwerionenforschung" (GSI) in Darmstadt is a heavy ion, fixed target experiment designed to analyze the phase transition from confined hadron matter to a deconfined Quark-Gluon-Plasma (QGP) at high net baryon densities [1]. The CBM experiment is part of the Facility for Antiproton and Ion Research (FAIR) which will include the syncrotrons SIS-100 and possibly in the future SIS-300 (figure 1) with a circumference of 1.1km to provide the experiment with the ions for the nucleus-nucleus collisions with center of mass energies of up to 5GeV per nucleus. The heaviest ions used for the collisions will be gold ions. CBM aims at exploring the phase diagram of strongly interacting matter predicted by the Quantum Chromodynamic (QCD) theory at an net baryon density not yet reached by any other experiment.

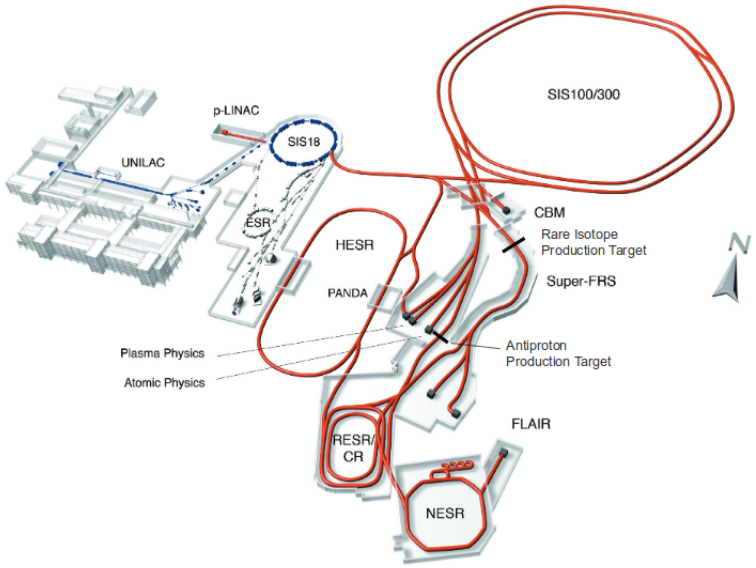

Figure 1: The FAIR complex at GSI which is currently under construction in Darmstadt. The sychrotrons SIS-100 and SIS-300 can be seen in the top right corner in red as well as the CBM experiment. The already existing synchrotron SIS-18 is displayed in the center of the picture colored in blue. Figure taken from [2].

To withstand the expected 10 million collisions per second, extremely pre-

cise and radiation resistent detectors are needed. As a free streaming system, CBM will avoid hardware triggers resulting in very high data rates. Thereafter, a high-speed data acquisition system is required to deal with the volumes of data from all the detector systems. The particle tracks need to be meticulously reconstructed, from the signals induced in the detectors, to discover which particles were present in the high density region at the time of collision. The best probes to analyze this state of matter are rare particles created in the collision which need to be filtered out. For a correct identification the Time of Flight (ToF) method is used which includes a diamond detector (T_0) that sits directly in the particle beam in front of the target with the ToF wall located about 10 meters behind the collision. This wall will cover about $120m^2$ with its active area and it is constructed with different types of multi gap resistive plate chambers (MRPC's). As a preparation for the CBM experiment a full-system test setup called mini-CBM (mCBM) was built in the already existing target hall at GSI and is part of the SIS-18 beam system. Here the different detector systems can not only test their existing modules but newly developed prototypes as well.

1.1 Physics of a Quark Glonen Plasma

In order to create a QGP within a nucleus-nucleus collision, high energy densities are needed. Large collider experiments such as ALICE at CERN in Geneva or STAR at the BNL in Brookhaven have very high center-of-mass energies and thus can create a QGP at temperatures much heigher than the critical temperature of $T_c \approx 156MeV$ but with net baryon densities close to zero. The QGP created with this method is very similar to the state of the Universe right after the big bang. To create a GQP at high densities fixed target experiments have been proven to be more efficient. With a fixed target experiment like CBM a QGP at moderate temperatures but high baryon densities with a critical density of about four times the normal baryonic density (ρ_0) can be created. The conditions created with this method are very similar to what is believed to be the state of matter on the inside of a neutron star and a neutron star merger.

There are two transitions expected when shifting from normal nuclear matter to a QGP. One such transition involves confined hadrons shifting to deconfined quarks and gluons the other is restoring chiral symmetry. So far indications point to the fact that both transitions happen simultaneously. However, the transition at high temperatures and low net baryon

densities appears to be a cross-over (continuous) while the transition at high net baryon densities and low temperatures appears to be a first order phase transition (discontinuous). This indicates that there must be a critical point of second order in between. To search for this critical point is one of the tasks of CBM. Other than the largely unknown properties of the phase diagram of QCD there are other questions concerning the QGP. Those include, but are not limited to, its viscosity, the equation of state and the speed of sound in a QGP. Additional exotic states of matter are predicted at high densities like a superconductor of QCD. Those features can be seen in figure 2 where the temperature is plotted against the net baryon density. It is a rough sketch of the phase diagram of QCD with most of its features only being theoretical hypothesis. Often the x-axis in phase diagrams of QCD use chemical potential, which is the energy needed to add another baryon to the nucleus, instead of net baryon density.

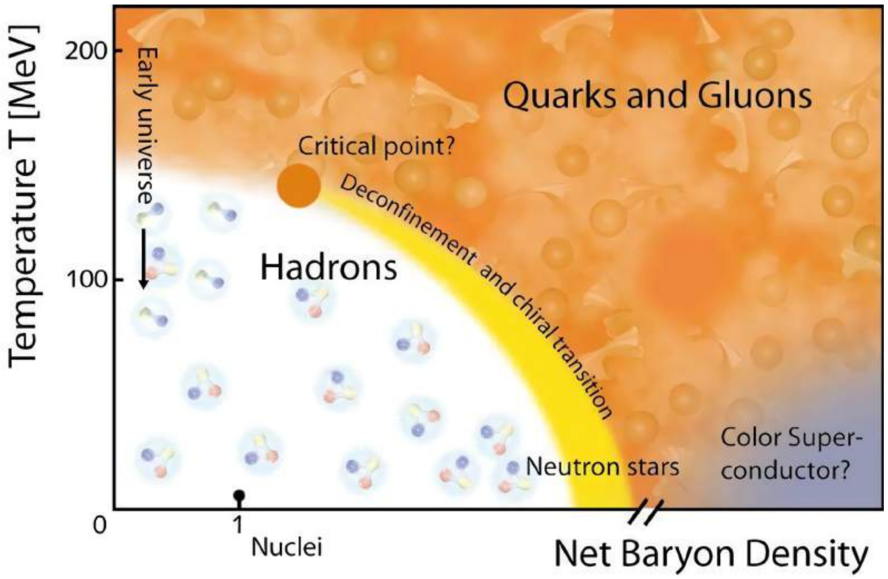

Figure 2: Phase diagram of QCD with temperature plotted against net baryon density. This is only a sketch and still largely unproven. Figure taken from [3].

At the beginning of a collision of two nuclei the highest energy densities are reached signaling the point where the particles with the highest rest mass are produced (figure 3, left). In case of the CBM experiment those

are strange quarks (95MeV). Later while the nuclei are overlapping mainly hadrons and thermal photons are produced (figure 3, center). After the freeze-out, which is the point where a thermal equilibrium is reached, only comparably light particles like kaons, protons, pions and lambda-mesons can be produced (figure 3, right). Over the whole process of the collision produced vector mesons decay into leptons which do not interact strongly. This helps to analyze every stage of the collision.

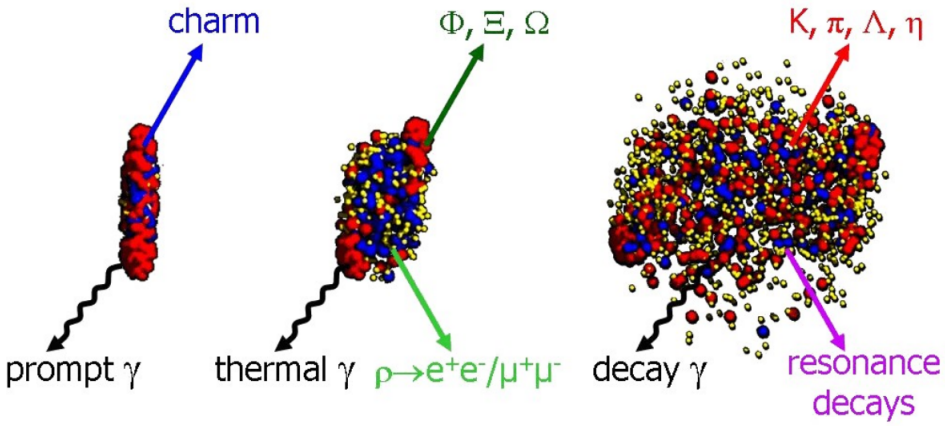

Figure 3: Model of two uranium nuclei colliding at 23AGeV. Initial collision on the left, nuclei overlapping in the center and a thermal equilibrium on the right. Figure taken from [4].

Although difficult to ascertain whether a nuclear collision resulted in a QGP or not there are a few indicators. QCD predicts that when a QGP expands and reenters the phase of confinement, particles that contain a strange quark are more likely to be produced (strangeness enhancement). [5] Since particles which contain strange quarks have a comparably long lifetime until they decay, their track is relatively easy to reconstruct when the decay products are detected. This enhancement has been the classic indicator for a QGP. However recent results have shown that strangeness enhancement also happens for hot matter that is not a QGP. [6] Another indicator which will be very important for the CBM experiment is sub threshold omega production. The omega baryon (Ω^-) contains three strange quarks and each strange quark has a rest mass of about 95MeV. To reach this point the energy from the primary collision is often not enough in CBM. Still omega baryons have been observed at those energies due to an accumulation of energy from sec-

ondary interactions. This is rather rare but with the high rate of CBM this could be a strong indicator for a QGP. A third indicator is that the production of J/ψ mesons is supposed to be suppressed in a QGP (J/ψ melting) due to their low binding energy which results in a recombining of the charm quarks to form D-mesons. Since charm quarks have a rest mass more than 13 times higher than strange quarks this effect will be hard to use in the CBM experiment. In order to verify those effects one needs a precise method to identify the particles produced in the collision. [7]

1.2 Time of flight

To properly identify particles with the time of flight method the rest mass and the charge need to be measured which, as each particle has a particular and unique combination when combined, are characteristic to each particle. Because most particles created in a high energy collision are unstable and decay before reaching the detector, their identification must be performed by analyzing their decay products and the reconstruction of their tracks. This method is only used for hadrons due to the fact that electrons and muons are almost at the speed of light when they reach the detector and the error on the time measurement is too large to distinguish them from one another. RICH detectors and calorimeters are more effective for their identification. The only charged hadrons with a lifetime long enough to reach the detectors are protons, pions and kaons. The rest mass cannot be measured directly but by measuring the momentum and the velocity of the particle the rest mass can be calculated. The momentum and the charge are measured by the curvature of the particle track in the magnetic dipole field. The velocity is calculated with the time of flight measurement (t_{tof}) and the distance to the vertex of the collision (L). Both of these measurements need to be done simultaneously in order to correctly identify the particles. [8] The relativistic equation for the momentum gives the relationship between the rest mass m_0, the velocity v and the momentum p:

$$p = \gamma v m_0 \tag{1}$$

By using the relationship for the velocity $v = L/t_{tof}$ and the lorentzfactor $\gamma = \frac{1}{\sqrt{1-\beta^2}}$ we can derive the relationship for the rest mass:

$$m_0 = \frac{p}{c}\sqrt{\frac{c^2 t_{tof}^2}{L^2} - 1} \tag{2}$$

In most cases including the CBM experiment the error of the rest mass squared ($\sigma_{m_0^2}$) is dominated by the resolution of the time of flight measurement σ_{tof} which follows from Gaussian error propagation for equation (2):

$$\sigma_{m_0^2} = \frac{2p^2 t_{tof}}{L^2} \sigma_{tof} \tag{3}$$

1.3 Multi-gap Resistive Plate Chambers

A Multi-gap Resistive Plate Chamber (MRPC) is a gas detector allowing precise time measurements of charged particles in heavy ion experiments. They consist of a large capacitor to which high voltage in the kV range is applied. Between the plates of the capacitor is a gas mixture which will be ionized if a charged particle passes through. Due to the electric field, the electrons and ions are drifting towards the electrodes of the capacitor after the ionization. The ions can be neglected due to their inertia. Prior to reaching the electrodes, the electrons ionize other atoms and start an avalanche of electrons. To stop the electrons from reaching the HV electrodes and thus discharging the capacitor, resistive plates are in their path. When an electron avalanche hits the resistive plates the electrons drift through the plate to recombine with the positive ions. This process prevents a spark from being created and reduces the dead time that results from a capacitor having to recharge as it would in a spark chamber. In order to get a good resolution, the gap size should be rather small (usually in the hundred micrometer range). This small size and corresponding decrease in the volume of gas with which the particles can interact decreases the efficiency of the detector. To increase the efficiency, multiple gas gaps separated by additional high resistive plates are used. In this way, the gap size remains small but the gas volume is larger.

To detect a signal, multiple strip or pad electrodes are placed on both sides of the detector. The electron avalanches induce a signal in those electrodes in the mV range. This signal then propagates along the strip to both sides of the detector where it is read out by preamplifiers.

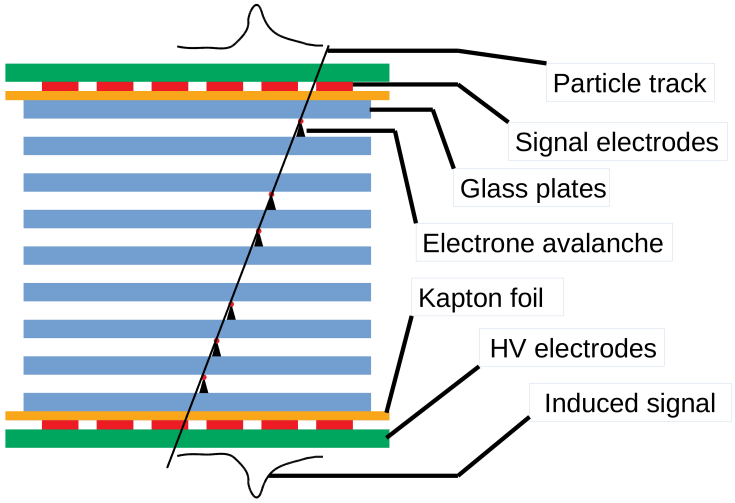

Figure 4: Particle passing through the multiple gas gaps in an MRPC and inducing a signal in the readout strip.

There are many different options when designing an MRPC, including material, gap size, gap number, gas mix, read out strip pitch to name a few. A deciding factor in the design is whether to use a symmetrical (figure 9) or asymmetrical (figure 4) configuration. The symmetrical design is essentially two asymmetric counters that share an electrode. This can provide the same field strength with only half the high voltage. Since the symmetrical design accelerates electrons in different directions a worstening of the time resolution is predicted but yet to be observed.

2 Experimental Setup

2.1 CBM

The CBM experiment is a dedicated heavy ion fixed target experiment with an interaction rate of up to 10MHz. This high interaction rate makes CBM unique compared to other competing experiments in a similar energy range like NICA (Nuclotron-based Ion Collider fAcility) or STAR (Solenoidal Tracker at RHIC). The high interaction rate leads to a higher production of rare particles like the omega baryon (Ω^-).

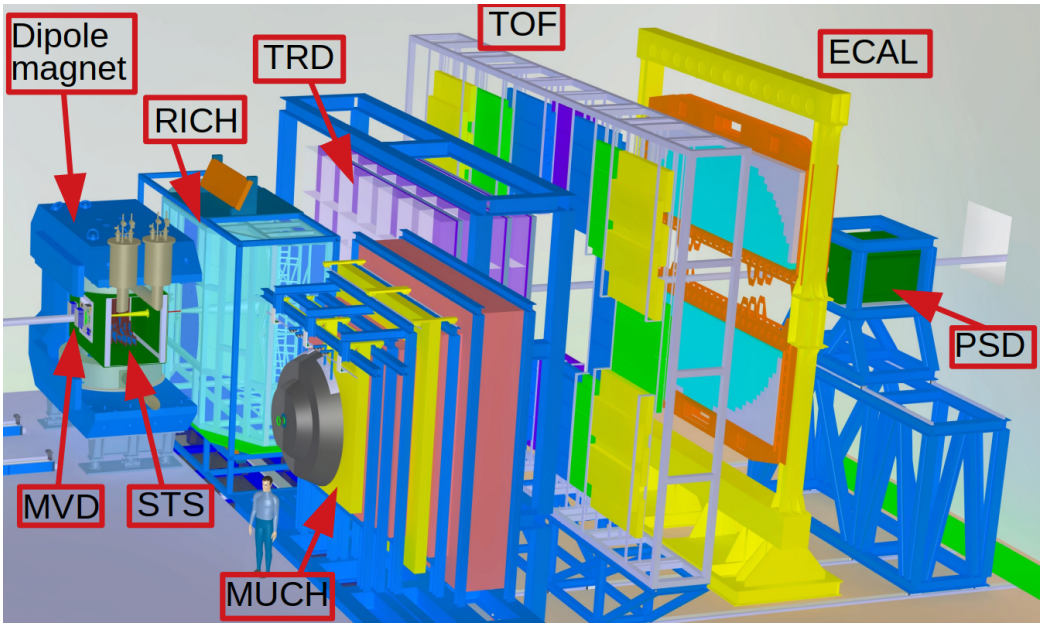

Figure 5: Model of the future CBM experiment with all the different detector subsystems. Figure taken from [9].

All the detectors which will be included in the CBM experiment can be seen in figure 5. The beam of gold ions enters from the left and strikes the target right before it enters the superconducting dipole magnet. In this magnet sits the Micro-Vertex Detector (MVD) to determine the position of secondary vertices and the Silicon Tracking System (STS) to measure the curvature of the particle track in the magnetic field for the momentum determination. Either a Ring-Imaging Cherenkov Detector (RICH) for electron detection or a Muon Chamber System (MUCH) for muon detection can be

used behind the magnet. These detectors will be put on rails and can be interchanged depending on the application. Next in the series of detectors is the Transition Radiation Detector (TRD) used for particle tracking and electron detection. The Time-of-Flight System (TOF) is used to provide precise time measurements of hadrons for particle identification. The Electromagnetic Calorimeter (ECAL) is used to identify and measure the energy of photons. The last piece of measurement equipment in the cave is the Projectile Spectator Detector (PSD) to measure the fraction of nucleons that did not interact with the target.

2.2 mCBM

Proposed in 2017, the mini Compressed Baryonic Matter experiment (mCBM) was designed as a CBM full system test setup. Located in the high-energy target hall at GSI, it was included in the accelerator system of SIS-18 in front of a beam dump. The purpose of this setup is to test the performance of the detectors for the CBM experiment and to see how well the different detector subsystems work together to reconstruct tracks. First run in 2018 and projected to run until 2021, this set up is expected to have parasitic beamtimes once a year. The goal is to be able to reconstruct Λ particle tracks and measure the exitation function of the Λ particle by 2021.

Figure 6 shows the schematics of the mCBM setup including all the detector systems mounted during the March 2019 beamtime. The diamond detector and the target are located on the left in the beam and all the other detector systems sit at a 25° angle to the beam direction. Consisting of two carbon ladders, the mSTS was installed behind the target and is followed by the mMuch system which used two GEM stations. The mTRD system had two stations mounted but due to readout problems it was not operational in this beamtime. The mTOF system containing five mTOF modules with 5 MRPC's each was located at 2.5m from the target. In order to find tracks with the mTOF system alone, a configuration of the modules was chosen to maximize the overlap of detectors. Therefore a double stack with two modules and a triple stack with three modules was set up as shown in figure 6. Behind the mTOF modules of the double stack other smaller detector prototypes were mounted for detector tests. The additional counters can be seen in figure 8. The mRICH detector consisted of one aerogel module which was mounted towards the end of the beamtime behind the triple stack.

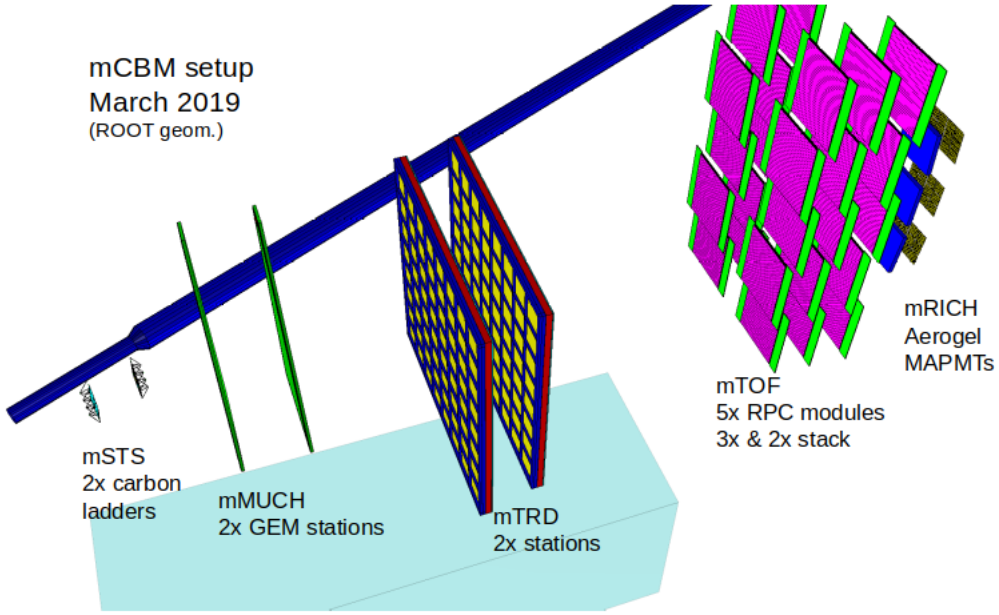

Figure 6: Model of the mCBM setup during the March 2019 beamtime. Figure taken from [10].

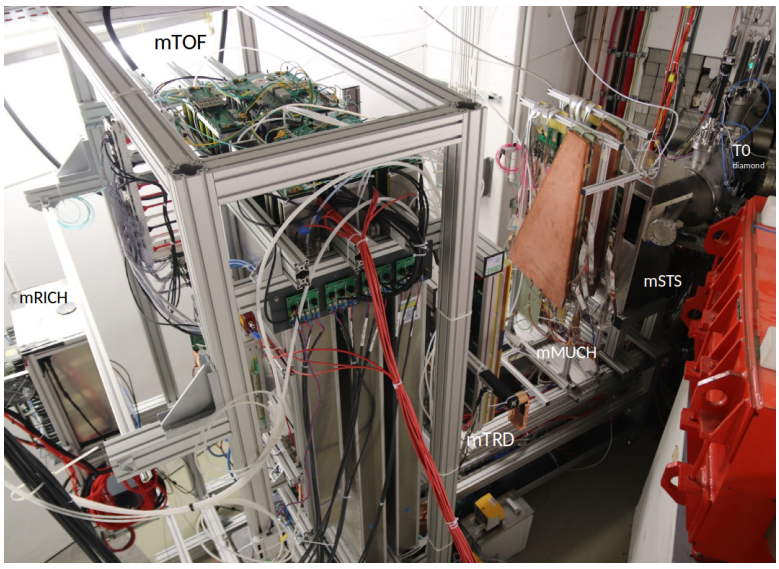

Figure 7: Experimental setup of the mCBM experiment during the March 2019 beamtime with all the mounted detector systems. Picture taken from [10].

Figure 7 shows a picture of the setup in the cave. The beam comes from the upper right corner and penetrates the diamond and the target. After the collision with the target all the produced particles spray into the cave. Only a fraction of the produced particles hit the detectors due to the acceptance of each layer. The additional counters of the mTOF setup were mounted behind the double stack. They included one box with two multi strip MRPC's build by USTC right behind the double stack. The multi strip MRPC prototype built by CERN for which the results are presented in this thesis was mounted behind the USTC box. Under the USTC box eight small pad MRPC's built by ITEP were installed. After this picture was taken two other prototypes from the CBM TOF group in Bucharest were mounted underneath the pad detectors.

Because mCBM does not use a dipole magnet a momentum measurement is not possible and the PID with the time of flight method cannot be applied. MC simulations have shown that it is still possible to reconstruct Λ particles from their decay into a proton and a pion. When combining the energies of two random particles out of all particles detected a peak at the rest mass of the Λ particle should appear. For this only mSTS and mTOF are needed. The goal of mCBM in 2019 was to approach full performance for all detectors at the highest intensities. This is necessary for the reconstruction of Λ particles with mCBM by 2020 and 2021.

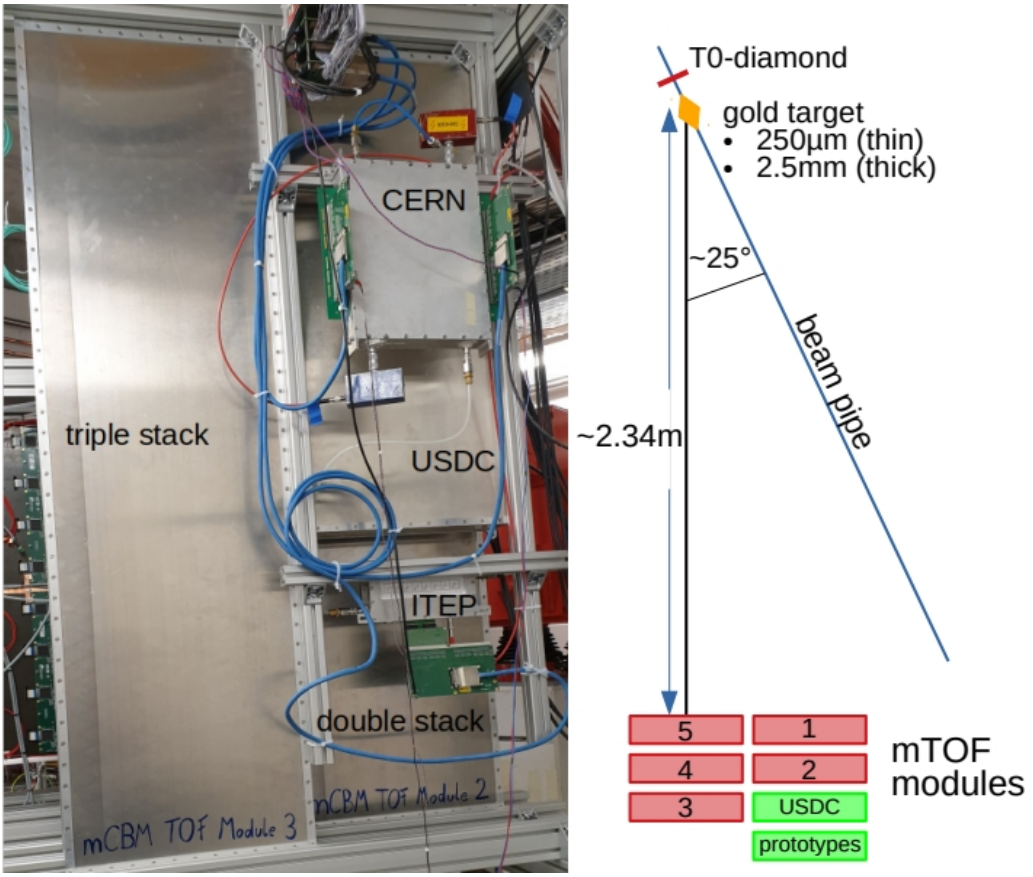

Figure 8: Left: The mTOF setup during the March 2019 beamtime. The last module of the triple stack can be seen on the left and the last module of the double stack on the right. Behind the double stack four prototypes (Bucharest module missing in this picture) are mounted for testing. Right: Schematic drawing of the location of the five mTOF modules and the additional prototypes.

2.3 Detector under test

High energy experiments like ALICE, STAR or HADES use MRPC's for TOF applications to capitalize on their low production cost for large areas and yet they can reach a time resolution below 50ps. The detectors used in those experiments need a rate capability for moderate charged particle flux below $1kHz/cm^2$. However since CBM is a fixed target experiment the rate will be much higher and thus detectors that can handle a charged particle flux of up to $10kHz/cm^2$ for the outer part of the TOF wall and up to $30kHz/cm^2$ for the inner wall are required. The rate a MRPC can handle is directly dependent on the resistivity and the thickness of the material used for the resistive plates. It has been shown that a lower resistivity and thinner materials increase the rate capability as well as thinner gas gaps. To lower the resistivity one can either increase the temperature of the material or simply use a material with a lower resistivity. Since controlling and stabilizing the temperature of multiple layers in a $120m^2$ wall is not applicable and gas gaps which are too small decrease the efficiency, alternative materials to the currently used soda lime glass which has a resistivity of $1.9 \cdot 10^{12} \Omega cm$ at 21°C are being tested. The CBM-TOF group has already built and tested MRPC modules using ceramic and low resistive glass for this reason. The disadvantage of those low resistive materials has been their minimal thickness. The low resistive glass has a thickness of $700\mu m$ and the ceramic has a thickness of $2mm$ compared to the soda lime glass with only $280\mu m$.

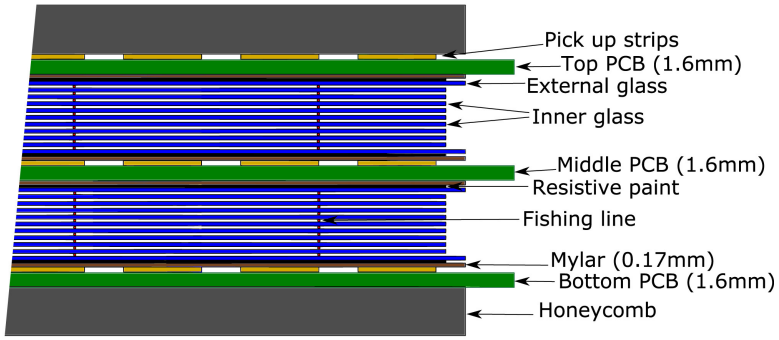

Figure 9: Cross-section of the CERN detector with its symmetrical design. Figure taken from [11].

The CERN prototype analyzed here also uses low resistive glass with

a resistivity of $3.8 \cdot 10^{10}\Omega cm$ produced in a float process. However, this glass only has a thickness of $400\mu m$ which makes it desirable for high rate applications. The low resistive glass separates the 20 $140\mu m$ gas gaps. Only for the two external glass layers in the symmetrical configuration soda lime glass was used. To space the gas gaps evenly, fishing line was put in between the glass plates. The two electrodes on the outside are positively charged while the shared electrode in the center is negatively charged. The gas mix used for all mTOF modules as well as the prototypes consisted of 95% 1,1,1,2 tetrafluoro ethane and 5% sulfur hexafluoride. The signals were read out by 18 20cm long strips with a pitch of 1cm. Eight of those strips had a width of 9mm and 10 strips had a width of 7mm. This detector has been tested before and has shown an efficiency of 98% at $\pm 9.2kV$ and a time resolution of 32ps. [11],[12] The CBM TOF group was hoping to duplicate those results at mCBM which would make the thin float glass a strong alternative to the currently used materials.

	CERN detector
material	low resistive flot glass
material thickness	0.4mm
resistivity	$3.8 \cdot 10^{10}\Omega$cm
gas gap number	20
gas gap size	0.14mm
strip number	18
strip length	20cm
strip width	7mm/9mm
strip pitch	10mm

Table 1: Design properties of the CERN detector

2.4 Readout chain

The read out of the CBM experiment will be free-streaming without any hardware triggers. CBM will have over 100,000 channels with rates up to 300kHz per channel. This combined with the need of extremely accurate time resolution puts very hard constraints on the data acquisition. To test the read out chain mCBM is also free streaming but it is still subject to constant changes and improvements. The following will give an outline on its status during the beamtime in March 2019. The analogue signals induced in the detector strips only have an amplitude of a few millivolts. To amplify the signal and discriminate actual signals against noise, the mTOF modules as well as most of the prototypes built by the CBM TOF group use the PADI10 (Pre Amplifier and DIscriminator) chip to read out all the detector strips. For comparison the ceramic pads from ITEP used the NINO ASIC (Application Specific Integrated Circuit) developed at CERN for the ALICE experiment. The NINO ASIC is also being used for the CERN detector since it was build at CERN, as well. If a signal reaches a certain threshold set in the PADI10/NINO it is converted into a unified rectangular signal with the starting and end time of the signal. One NINO chip as well as the PADI10 chip has eight channels and one board has 4 chips. This means in order to read out the 32 channels on both sides

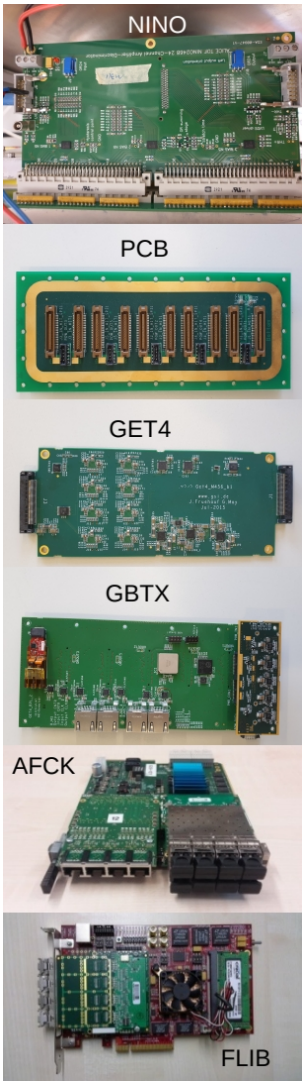

Figure 10: All the components of the readout chain. Pictures partly taken from [8].

of the CERN detector two NINO boards are needed. However, NINO has a much higher amplification than PADI10 which results in a different ToT spectrum. After the preamplifier/discriminator the signal travels through a feedthrough PCB (Printed Circuit Board) to the TCD (Time to Digital Converter).

The mCBM experiment uses a GET4 (Gsi Event-driven Tdc) chip which combines 4 channels, digitalizes the data into a 32-bit number and determines the arrival and the end time of a hit by comparing the signal from the PADI10/NINO to its internal clock of 160MHz. In order to get a precise measurement in the order of picoseconds 160MHz is not enough and a signal delay chain is used to increase the binning of the internal clock. This is done on both sides of the detector strips and to get the best estimate of the arrival time t_0 at which the particle crossed the detector the average of the arrival times on each side of the strip t_{left}, t_{right} is used in order to average out the position of the hit:

$$t_0 = \frac{t_{left} + t_{right}}{2} \tag{4}$$

To have a measurement which is proportional to the charge deposited, the time difference t_{Tot} between the arrival time t_0 and the end time of the signal is used. In the coordinate system used the x-axis runs across the read out strips and the y-axis runs along the strips. This way the X coordinate of the hit is simply the position of the strip. The y coordinate is calculated with the signal velocity v_D by looking at the time difference at which the signals arrive at the readout:

$$Y = (t_{left} - t_{right}) \cdot \frac{v_D}{2} \tag{5}$$

A GET 4 board contains eight GET4 chips. The measurements made by five GET4 boards are then collected, combined and converted in a GBTX ASIC to an optical fiber link. From here the data goes to the AFCK board which is an FPGA (Field Programmable Gate Array) to build micro time slices (small data packages of events at similar times) with the collected data from up to six GBTX boards. Those micro time slices are then sent via optical transmission to a FLIB (First Level event selector Interface Board) which combines micro time slices into time slices and stores them in a TSA file.

3 Data Analysis

In order to analyze the data from mCBM all the TSA files were stored on the GSI Kronos workstation. Since this is a free streaming system this data contains a lot of noise. To filter out the actual events and find particle tracks the following steps are taken.

3.1 Unpacker

Using a script called `startMQ_Mcbm.sh`, an Unpacker filters actual events from background noise and saves it in a .root file. Unpacking means building events that fit certain parameters that can be set freely. The event building works as follows. All the data is available and if a hit (a hit is a signal on a detector strip which has been detected on both sides of the strip) was detected a time window starts. If all the required detectors have a hit in this time window it is considered a real event. If not, it is regarded as noise and not saved. The size of the time window as well as the required detectors are chosen in the script. Experience has shown that strict limits on the data show the best results. For the efficiency analysis a time window of 50ns was chosen in which 10 detectors out of the full mTOF setup had to show a hit. For the rate analysis a time window of 50ns was chosen in which only one detector out of the full mTOF setup had to show a hit. The data which was kept is then calibrated in the next step.

3.2 Calibration

If one sees a correlation between two properties in the measurement even though no correlation is wanted the bin-by-bin method is used to get rid of those correlations. This improves both the efficiency as well as the resolution measurement. The bin-by-bin method examines every bin in a two-dimensional histogram, calculates the mean of this bin and shifts the bin so the mean now sits at a constant value (mostly 0). This calibration includes measurements of position, Time Over Threshold (TOT), and walk effect. All of this is done by the calibration scrip `calib_batch.sh`. The results from this calibration include a first estimation for the resolution and an overview over the different calibration steps for every detector.

The position calibration is necessary because the cables of the different channels have a slightly different length. That causes the position of the

strips to be also slightly shifted in the measurement. Figure 11 shows a picture of the calibrated and uncalibrated position measurement. Here the y position of a hit is plotted against the strip number so that the red area represents the active area of the detector since the counts are visualized by the color on a logarithmic scale. The left picture is taken before the first calibration iteration, so the scale is still a lot larger because some of the hits were measured outside the active area of the detector. Those are nonphysical events and they are caused by reflections due to different impedances in the readout and those events need to be filtered out. Even on such a large scale one can see that the means of the strips do not sit on equal values. The right picture now shows the calibrated position measurement. This can now be interpreted to be the active area of the detector where every bin on the x-axis corresponds to one strip of the detector and every bin of the y-axis corresponds to one centimeter in strip length.

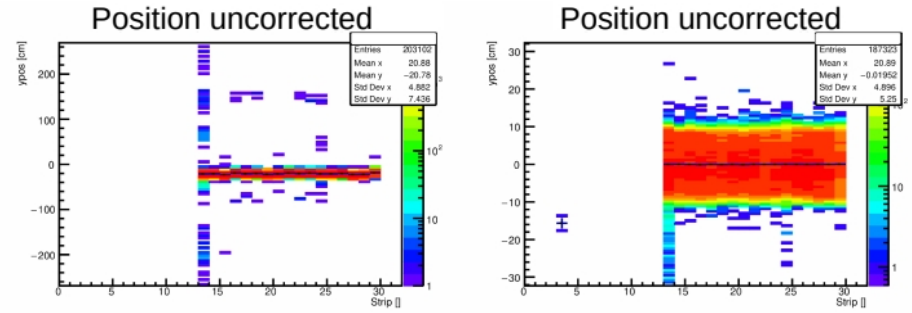

Figure 11: Before (left) and after (right) the position calibration.

The next calibration step takes the use of different amplifiers into account which results in different Tot's. In figure 12 the x-axis corresponds to the strip number and the y-axis corresponds to the Tot after the preamplifier, the color coding is again the number of hits on a logarithmic scale. The mean of the Tot is shifted to 5 since 0 would be nonphysical for a time difference. Also, the values around the mean get clinched so that after the calibration there is a standard deviation over a factor 10 lower than before.

The walk correction takes the shift of the arrival time for different signal heights into consideration. A larger signal has a steeper increase and thus reaches the necessary threshold to trigger a signal faster than a smaller signal. That means the hits with a smaller Tot actually occur earlier than measured at the readout. This effect is called walk and it can be corrected the same

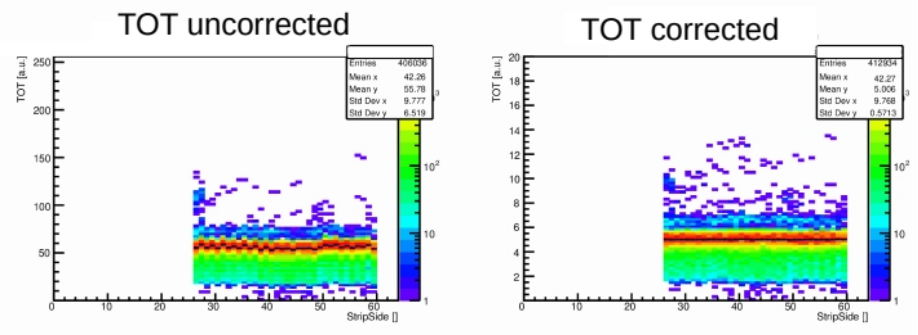

Figure 12: Before (left) and after (right) the TOT calibration.

way as the other steps were corrected with the bin-by-bin method. Figure 13 shows this with the x-axis corresponding to the logarithm of the Tot. The y-axis is the time difference between the arrival times at the detector under test and the reference counter. In the uncorrected picture on the left in figure 13 this time difference is larger for small Tot's. The corrected picture on the right now has a leveled distribution around 0 as requested. The low populated bins are not corrected since that would improve the measurement artificially.

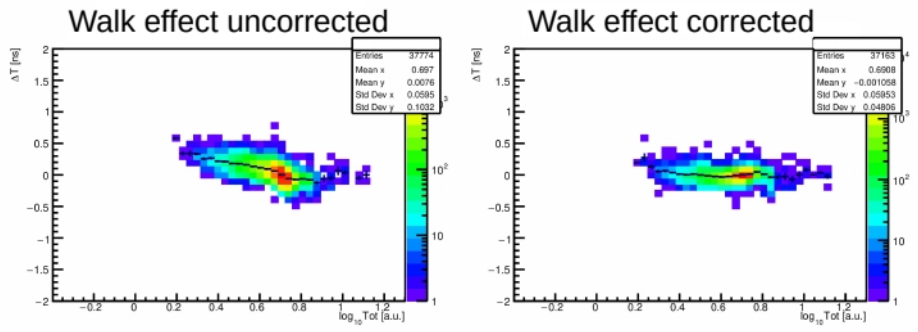

Figure 13: Before (left) and after (right) the walk calibration.

3.3 Tracker

All the calibration steps are done for every detector and afterwards the tracker tries to combine this data and reconstruct a particle track. In addi-

tion, the tracker script `iter_tracks.sh` produces the efficiency and resolution of the chosen Detector under test (DUT). For this analysis the CERN detector was chosen as DUT and the diamond plus the two detectors in the double stack that were in front of the CERN detector were used as reference counters. In this case the efficiency (ϵ) was approximated by comparing tracks every detector saw (N_4) to tracks every detector except the DUT (N_3) saw. This process can be seen in figure 14 where the active area of the detectors is displayed that participate in the tracking. The top row is the diamond counter, the second row is the first module in the double stack, the third row is the second module in the double stack and the bottom row is the CERN detector. Only the efficiency of the DUT can be taken seriously since the others are requested in the tracking and thus biased. The left column of pictures are the four hit tracks, the center column are the three hit tracks and the right column is the calculated efficiency with formula 6.

$$\epsilon = \frac{N_4}{N_4 + N_3} \tag{6}$$

The resolution can be derived with the χ^2 method from the reconstructed particle tracks. In order to prevent fitting a track through hits which did not come from the same particle a χ^2 limit for time and space is chosen to cut residuals that are above a reasonable value. For every hit in the DUT that was part of a four hit track the residual is taken. All of the residuals are then put into a histogram where a gaussian fit is applied. The sigma of this fit corresponds to the time resolution.

3.4 Track Evaluation

The `eval_tracks.sh` script only looks at events including the closest reference counter and the detector under test. After it found a hit in the reference counter it looks to the DUT counter and evaluates which hit fits best to the hit on the reference counter. It then calculates the time difference between those hits. This reduces the errors on the time and space resolution and gives a more precise measurement with a better resolution.

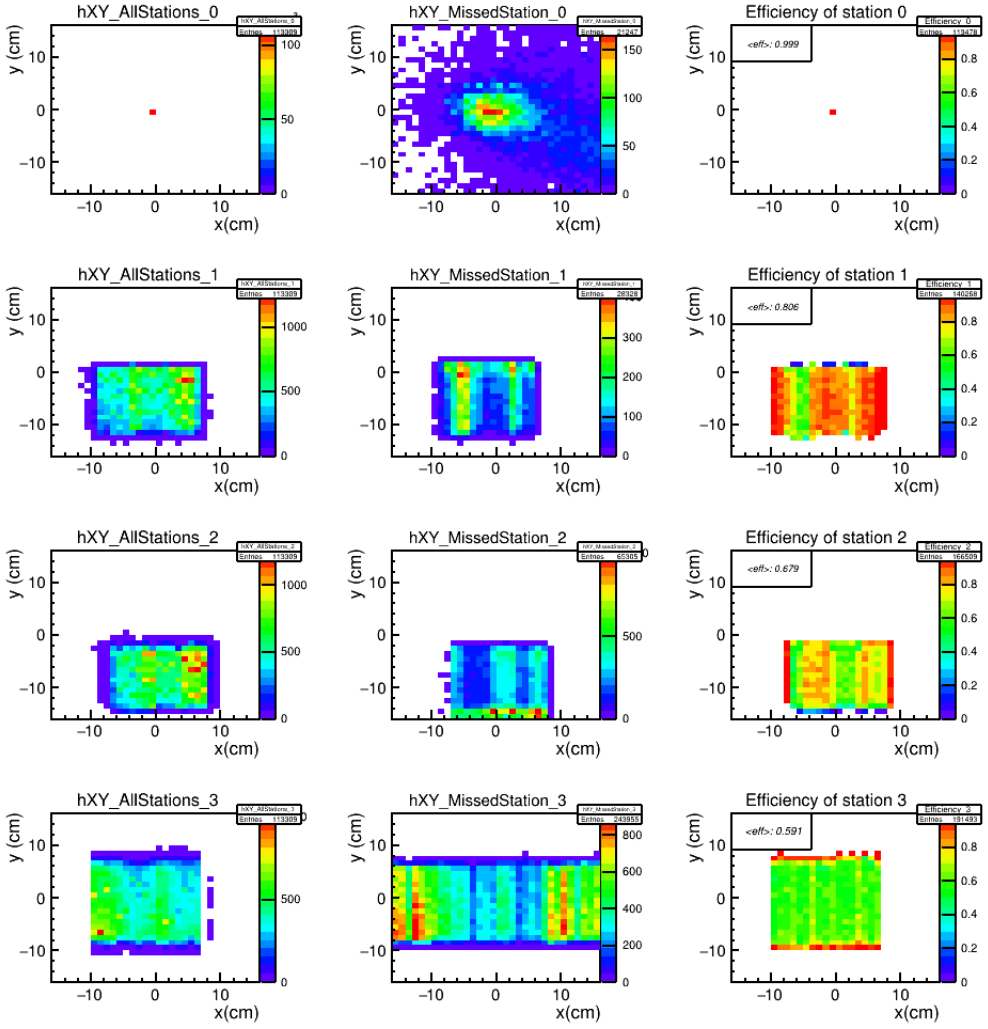

Figure 14: Example of the efficiency approximation. The first three columns are reference counters and the fourth row is the detector under test. The left column are four hit tracks, the center column are three hit tracks and the right column is the calculated efficiency with formula (6).

4 Results

To analyze the performance of the CERN detector the focus was put more on the efficiency rather than the resolution due to the fact that the resolution seemed to be in an acceptable range but the efficiency showed a problematic behavior early on. During the March 2019 beamtime at mCBM the beam conditions in the cave were not fully optimized yet. The main problem was hitting the center of the target with the beam. Solving this resulted in less actual beamtime and less data than expected. The most stable conditions were reached on the final day (March 30th) of the beamtime. On this day a few ten minutes runs were done at what was believed to be a moderate rate. During those runs, detector tests like high voltage scans and threshold scans were possible for each detector subsystem individually. After that a rate scan was performed starting at the lowest rate possible and subsequently increasing the intensity of the beam and the target thickness until the highest possible rate was reached.

4.1 High Voltage scan

During the runs at which detector tests were possible a high voltage scan was performed for the CERN detector. With an increase in high voltage the efficiency of a MRPC goes up because more electrons from ionization result in an electron avalanche big enough to be detected. However, this also results in a higher dark rate due to free electrons which were not ionized by particles from the collision. Those electrons also get accelerated and induce a signal. At rather low voltages the efficiency increases a lot as the voltage is slightly increased. After the detector is above 90% efficiency the increase saturates even as the voltage further increases. Here one has to be careful because the highest high voltage allowed is limited by the detector design. If this is ignored and the high voltage is increased above this point a spark can occur in the detector, that can possibly damage the resistive plates and the read out electronics. Even if no damage is done by a spark the electrodes need to be recharged afterwards which results in a deadtime of the detector. The voltage at which the efficiency stops to increase and goes into saturation is the ideal working voltage for an MRPC. From previous measurements the working voltage of the CERN detector was believed to be at $+9kV$ for the two anodes and $-9kV$ for the cathode. This is further noted to be $\pm 9kV$. The steps for the high voltage scan were $\pm 8.5kV$, $\pm 8.75kV$, $\pm 9kV$, $\pm 9.3kV$

and $\pm 9.4kV$.

The results from the high voltage scan can be seen in table 2 and the blue curve in figure 15 where the efficiency is plotted against the applied voltage. For all voltage settings the efficiency stayed between 20% and 50%. This differs strongly from the expected result and what had also been measured previously where the detector showed an excellent efficiency of 98%. The curious thing about the curve is, however, that there still seems to be a saturation at higher voltages even though the efficiency is below 50%. Such a saturation would usually not occur if the detector was anywhere below 90% efficiency. This could indicate that the detector itself was in fact at above 90% effective but that somehow data got lost in the readout electronics. No systematical errors were included in this plot since there seems to be a very large unknown systematical error that needs further investigation. The statistics from the ten-minute runs were so large that the statistical error is smaller than the points in the graph. For comparison, two measurements with the same detector from the cosmic stand in the laboratory in Heidelberg were included into the plot (orange curve).

run	high voltage	efficiency	counter rate (Hz)
144	9.3kV	43.1%	$(8.5 \pm 1.1) \cdot 10^4$
146	9.4kV	44.0%	$(7.4 \pm 0.9) \cdot 10^4$
148	9.0kV	38.4%	$(5.8 \pm 0.4) \cdot 10^4$
149	8.75kV	32.0%	$(4.7 \pm 0.8) \cdot 10^4$
150	8.5kV	22.9%	$(2.7 \pm 0.5) \cdot 10^4$
HD1	9.0kV	58.1%	cosmic muons
HD2	9.2kV	68.5%	cosmic muons

Table 2: Overview of all runs used for the high voltage scan and the corresponding efficiency.

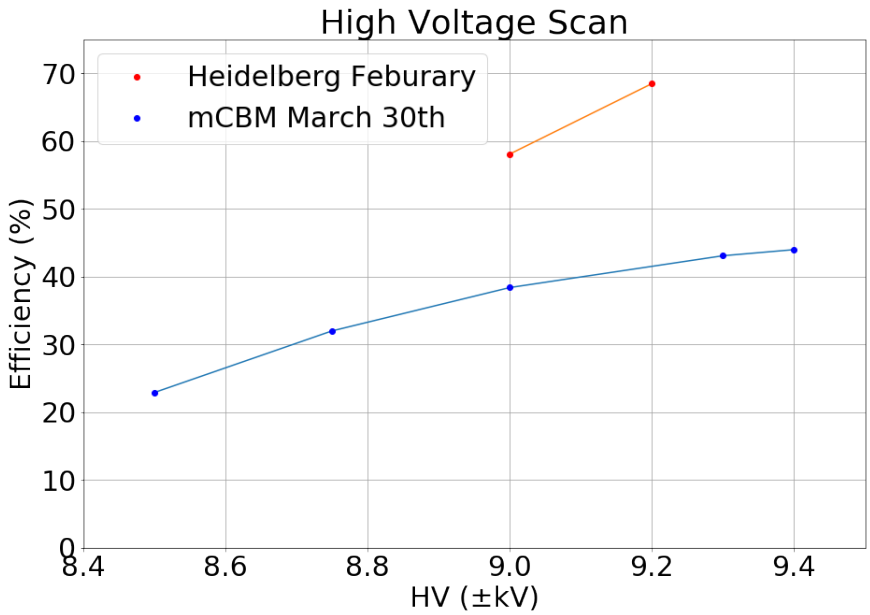

Figure 15: High voltage scan at mCBM (blue curve) and two data points from the cosmic muon stand in Heidelberg (orange curve)

4.2 Rate scan

Since the efficiency of the detector did not show the expected result the rate dependency of the efficiency was investigated. The thin low resistive glass in the detector should make the detector performance independent of any rate changes. If a rate dependence is measured, a data loss in the read out chain is indicated. This means the detector itself was at a high efficiency but the GET4, the GBTX, the AFCK or the FLIB had had so much data intake that an internal buffer got filled up and any additional data got lost until the buffer got reset and new data could have been saved. A similar effect has already been observed in some mTOF modules. Another already known problem is the GET4 having problems synchronizing with the external clock of the read out. This results in four channels being dead until synchronization is restored. However, this leaves a very recognizable pattern in the efficiency measurement with exactly four channels not being efficient. This pattern was not observed for the CERN detector as displayed in figure 14 where the active area in the bottom right shows a homogeneous efficiency without any

four channel patterns.

The high voltage of the detector was set to ±9.3kV for the rate scan. Different intensities and target settings were chosen for nineteen different runs out of which ten were selected that showed a stable rate. For those ten runs the beam had five different beam intensities with each intensity having one run with a thin $250\mu m$ target and one run with a thick $2.5mm$ target. An overview of the runs and their settings can be seen in table 3. The information about the target as well as the intensity used for a run was given by the beam control at GSI. The beam during this beamtime consisted of silver (Ag) ions. A gold ion beam would have resulted in an interaction ratio of 1% for the thin target and 10% for the thick target as planned for CBM. However, since this was a parasitic beamtime the beam ions could not be chosen by mCBM. A silver beam results in a smearing of the interaction percentage, but the rate should still change by a factor of ten for a target change.

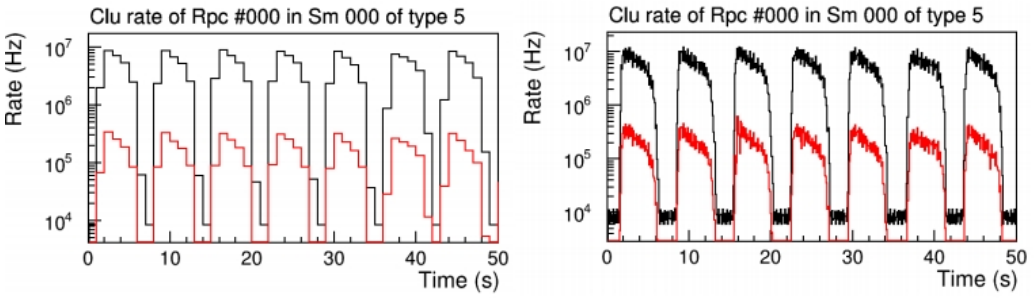

Figure 16: Rate measurement for run 166 with different granularity (left: 1s, right: 0.1s). The diamond rate is displayed in black and the CERN counter rate is displayed in red.

The rate was measured by unpacking the raw data with only requiring one hit in any detector for it to be considered an event. That means every signal detected on both sides of a strip is kept. The number of events is then counted and filled into a separate histogram for every detector. This was done with a binning of 1 second as well as with a binning of 0.1 seconds. An example of this can be seen in figure 16 taken from run 166. The black histogram is the rate on the diamond counter and the red histogram represents the rate on the CERN detector. Here one can see the spill structure of the beam with an on-spill time of about four seconds and an off-spill time of about two seconds. Neither the 1s nor the 0.1s binning indicates any data loss. The

rate was then calculated by taking the mean of all the maximum rates per spill.

First this was done for the diamond rate since the diamond was used as a reference counter in all the efficiency measurements. The results can be seen in figure 17 where the diamond rate is plotted against the run number. At lower intensities it can be seen that the intensities measured align with the values given by the beam control (table 3) for the first four runs. After that the rate measured on the diamond seems to go into some kind of saturation due to the high rate. After run 165 the rate appears to stay on the same level even though the beam intensity got increased further. At the end it even seems to drop a little for run 172 and 173. This happened because those were the two runs with the highest intensities of all and at that point the spills could not be clearly identified in the histograms anymore which lowers the value and increases the error of the mean in the algorithm.

It is also worth mentioning that the diamond sits in front of the target which means that the measurement of the diamond rate should be independent of the target change. This is also verified in figure 17.

run	target	proposed rate (Hz)	measured rate (Hz)
159	thin	$2 \cdot 10^5$	$(1.9 \pm 0.3) \cdot 10^5$
160	thick	$2 \cdot 10^5$	$(1.7 \pm 0.4) \cdot 10^5$
162	thin	$3 \cdot 10^6$	$(2.2 \pm 0.7) \cdot 10^6$
163	thick	$3 \cdot 10^6$	$(2.3 \pm 0.5) \cdot 10^6$
165	thin	$2 \cdot 10^7$	$(8.1 \pm 1.1) \cdot 10^6$
166	thick	$2 \cdot 10^7$	$(7.9 \pm 1.3) \cdot 10^6$
168	thin	$4 \cdot 10^7$	$(8.7 \pm 1.9) \cdot 10^6$
169	thick	$4 \cdot 10^7$	$(9.0 \pm 1.1) \cdot 10^6$
172	thin	not given	$(6.0 \pm 1.2) \cdot 10^6$
173	thick	not given	$(5.3 \pm 3.1) \cdot 10^6$

Table 3: Overview of all runs used for the rate scan and their proposed and measured beam rate.

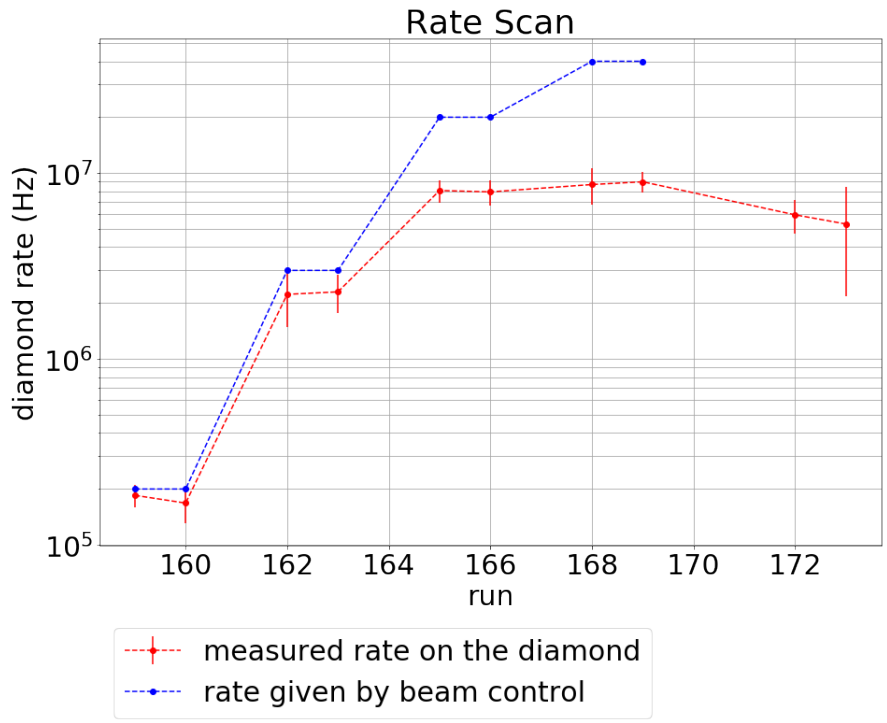

Figure 17: Difference between proposed and measured beam rate.

The next step was to compare the rate on the CERN detector to the measured efficiency. The results of this measurement can be seen in table 4 and figure 18. As expected the rate on one single detector is much lower than the rate on the diamond because a detector only covers a small fraction of the angular space behind the target. Furthermore, not every beam particle interacts with the target. A clear spill structure can still be seen in figure 16. Since the detector sits behind the target the rate should increase by the thickness of the target, rusulting in a factor of ten when changing from the thin to the thick target as the intensity stays the same. However, this is not what the data indicates. The target changes between run 159 and 160, 162 and 163, 165 and 166 and also partly between 172 and 173 (hard to say due to the large error on 173) all show that the rate only increases by a factor roughly between two and three. This can possibly be explained if the beam did not hit the target perfectly and interacted with other matter like the beam pipe as well. A clear saturation of the rate as seen for the diamond rate cannot be seen here. When looking at the efficiency a dependency between rate and efficiency can clearly be observed for both targets since the efficiency drops from almost 60% at the lowest rates to below 25% for the highest rates. What at first seems counter intuitive when arguing with data loss that results in efficiency loss at high rates is the fact that the runs where the thick target, which results in a higher rate was used, showed a significantly higher efficiency than the runs where the thin target was used.

run	target	counter rate (Hz)	efficiency
159	thin	$(2.5 \pm 0.4) \cdot 10^3$	49.7%
160	thick	$(5.6 \pm 1.2) \cdot 10^3$	59.1%
162	thin	$(2.9 \pm 0.8) \cdot 10^4$	44.2%
163	thick	$(8.0 \pm 1.8) \cdot 10^4$	52.8%
165	thin	$(1.1 \pm 0.2) \cdot 10^5$	23.1%
166	thick	$(2.9 \pm 0.5) \cdot 10^5$	38.2%
168	thin	$(9.4 \pm 2.4) \cdot 10^4$	22.6%
169	thick	$(2.8 \pm 0.4) \cdot 10^5$	45.2%
172	thin	$(3.6 \pm 0.6) \cdot 10^5$	20.5%
173	thick	$(6.0 \pm 3.7) \cdot 10^5$	23.6%

Table 4: Overview of all runs used for the rate scan and the rate on the counter with the corresponding efficiency.

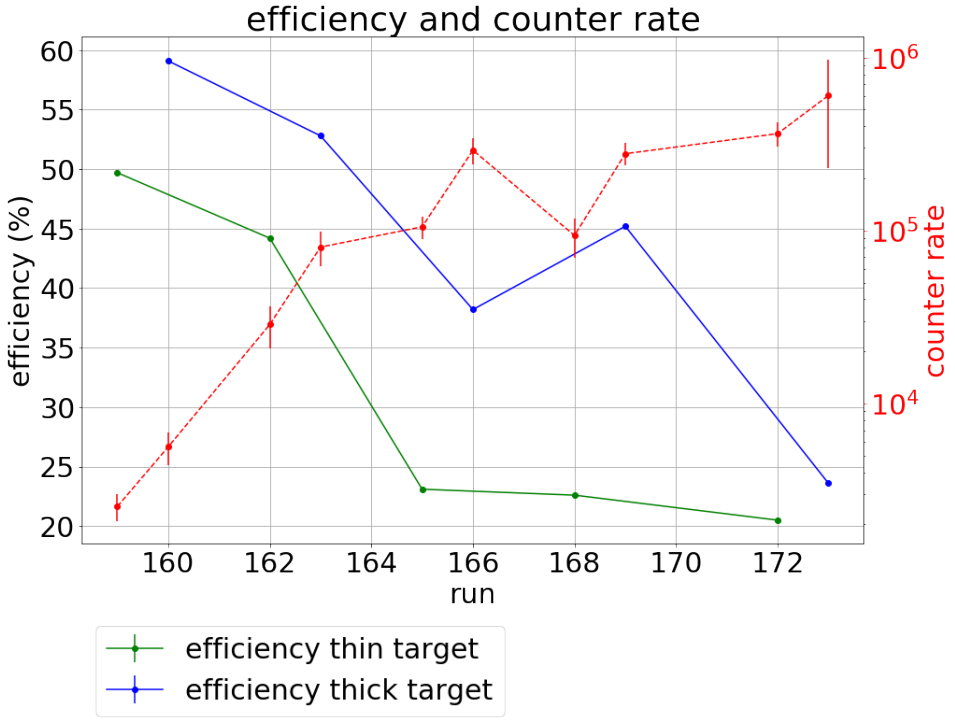

Figure 18: Correlation between counter rate and counter efficiency.

This strange effect was possibly an artifact due to the extrapolating tracking setup. Since the detector under test was the last detector in the setup it is possible that particles that induced a signal in the diamond and the double stack got absorbed (for example in the USTC box) and did not reach the CERN detector. This was a problem independently of the target thickness. However, mCBM FLUKA simulations have shown that a significant amount of secondary electrons (delta electrons) were not only produced in the collisions but also travelled far enough to possibly induce a signal in some detectors. [13] Those secondary electrons are produced when high energy ions simply knock the electrons out of their shell. Those electrons can be very fast with an energy of a few hundred keV. Usually those particles can be easily identified when traveling through a magnetic field, but this was not possible here since mCBM did not use a dipole magnet. Delta electrons can be very easily absorbed by any matter in their path, which means that there were many more of those electrons present compared to the hadrons produced in the collision when using a thin target because most of the electrons were absorbed in the thick target. There was no other detector system mounted directly in between the target and the double stack so no other matter (other than air) stopped those electrons from reaching the double stack, inducing a signal in the first detectors, get absorbed in the USTC box and never reaching the CERN prototype. This would lower the efficiency of the CERN detector since there would be no particle anymore to detect. Since the ratio of delta electrons to hadrons coming from the thin target is higher than for the thick target this might explain the efficiency discrepancy between the two targets. To investigate how much impact the delta electrons actually had, further simulations are needed.

Furthermore the rates during the high voltage scan were analyzed and it turned out the rate was not as stable as expected. For the five runs used for the high voltage scan the rate on the detector fluctuated between $2 \cdot 10^4$Hz and $9 \cdot 10^4$Hz. During the high voltage scan the detector was at 43.1% with a high voltage of $\pm$9.3kV and a rate of $(8.5 \pm 1.1) \cdot 10^4$Hz. This measurement appears to be consistent with the efficiency during the rate scan.

4.3 Rate vs. current

To find out if data got lost in the read-out chain, the rate was compared to the currents in the detector during the rate scan. In theory the currents should be proportional to the rate. The currents during all the nineteen runs of the rate scan can be seen in figure 19. This data was provided by the high voltage supply. Here it becomes clear why some of the runs were not used for the analysis due to low statistic or an unstable rate during the run. It is important to say that the currents for run 159 and 160 were so small that a good current measurement from those runs was impossible.

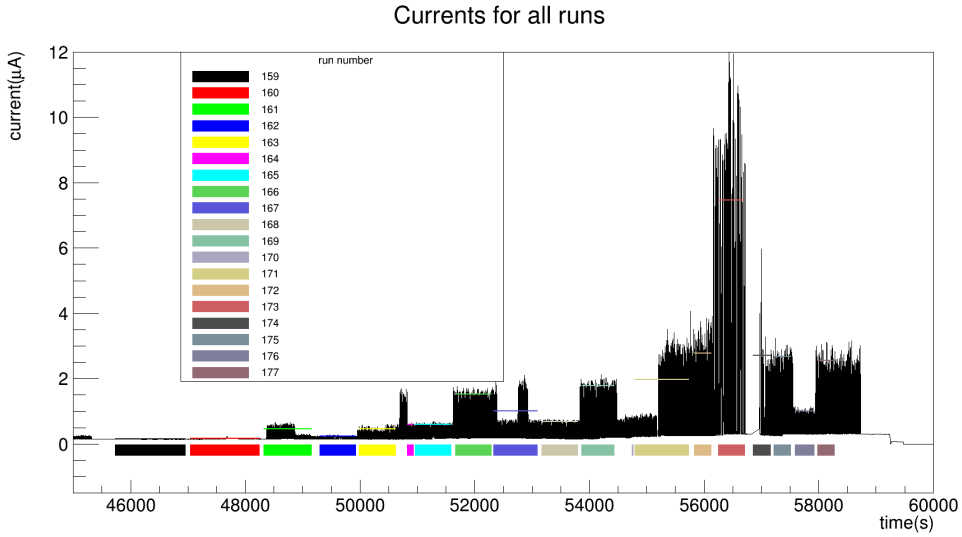

Figure 19: All currents measured during the rate scan with the average of every run.

To analyze the current data the same algorithm that analyzed the rates was used where the mean is taken from all the maximums of every spill. A picture of this can be seen in figure 20 for run 166. The error was then, again, the error of the calculated mean. In this plot also the spill structure can be seen but since the granularity was larger for this measurement it is not as clearly visible as it was for the rate.

In figure 21 the average spill height for all the runs is plotted in order to compare it the efficiency. This shows a very similar behavior to the rates in figure 18. Once again the target change does not scale with a factor of ten in the data which confirms the rate measurement. The average current of

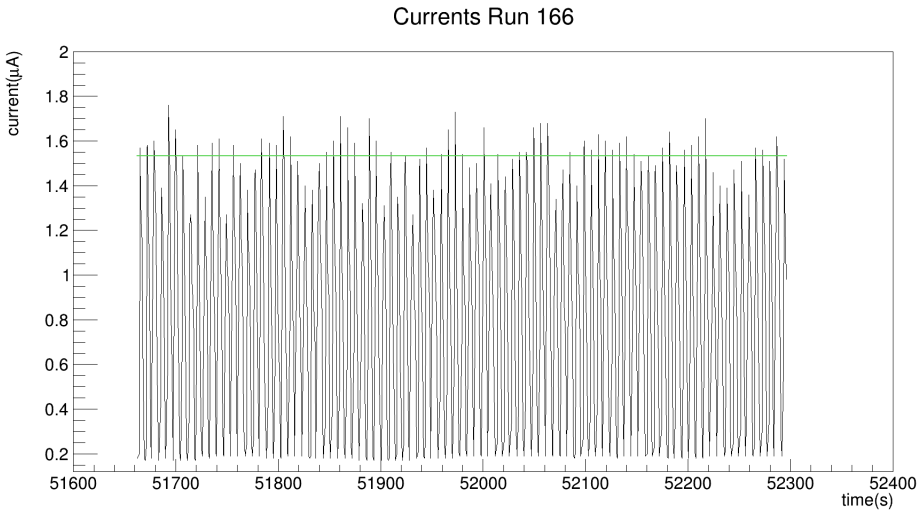

Figure 20: Currents during run 166 and the calculated average

Figure 21: Correlation between currents and counter efficiency.

$(6.89 \pm 2.14)\mu A$ measured during run 173 is also not very representative to the actual current when looking to figure 19.

To directly compare the currents to the rates they were plotted against each other in figure 22. Theoretically, this should show a linear behavior. It is hard to judge from this plot whether or not the behavior was linear due to the large errors on the high rate runs. Yet a small indication can be seen that for high rates the current increases more than the rates did which would support the argument for data loss in the readout. For further investigation the errors need to be adjusted. One way of doing this would be to correlate every entry in the current measurement to the corresponding rate and then check if this saturation can still be observed.

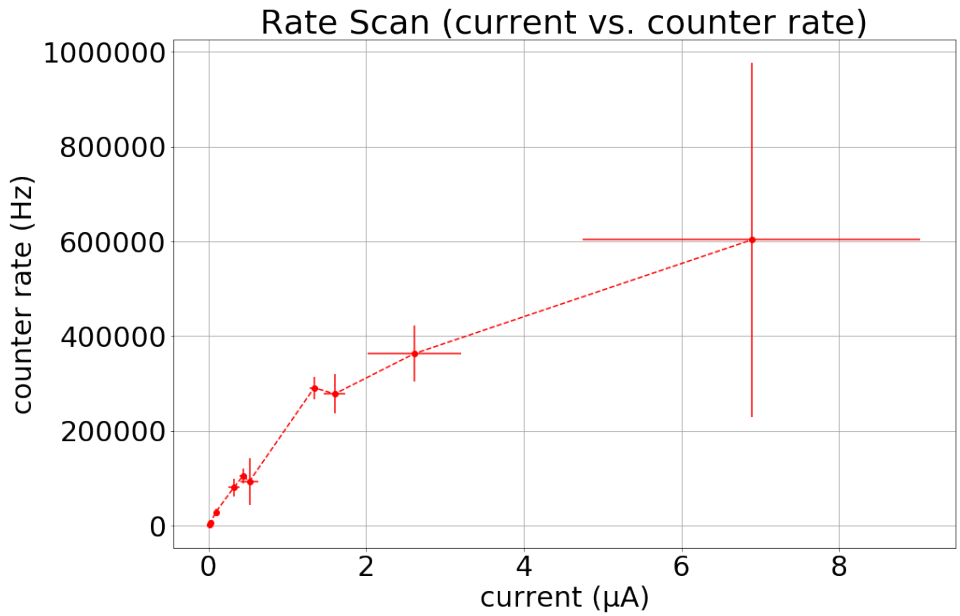

Figure 22: Average rate on the detector compared to average current in the detector.

4.4 Resolution

The main focus of this analysis was on the efficiency of the detector. In order to complete a full performance analysis the resolution of the detector is also included in the figures 23, 24 and 25. They show the time and space resolution of the detector during run 160 which showed the best efficiency out of all the analyzed runs from mCBM. Figure 23 shows the time resolution of (102.7 ± 0.3)ps. Figure 24 shows the spatial resolution in x-direction (across the strips) of (3.896 ± 0.009)mm. Figure 25 shows the spacial resolution in y-direction (along the strips) of (2.991 ± 0.012)mm. The time and the y resolution show a symmetrical gaussian peak while the x resolution has a one-sided shoulder that is not included into the fit for the resolution. This shoulder comes from the two different strip widths not implemented in the geometry used by the software and are therefor not corrected for. The time resolution of about 100ps is only roughly in the range of the expectation for the CBM experiment where resolutions below 80ps or even 50ps are needed. The spacial resolution fits very well with the expectations for CBM which is 3mm to 5mm.

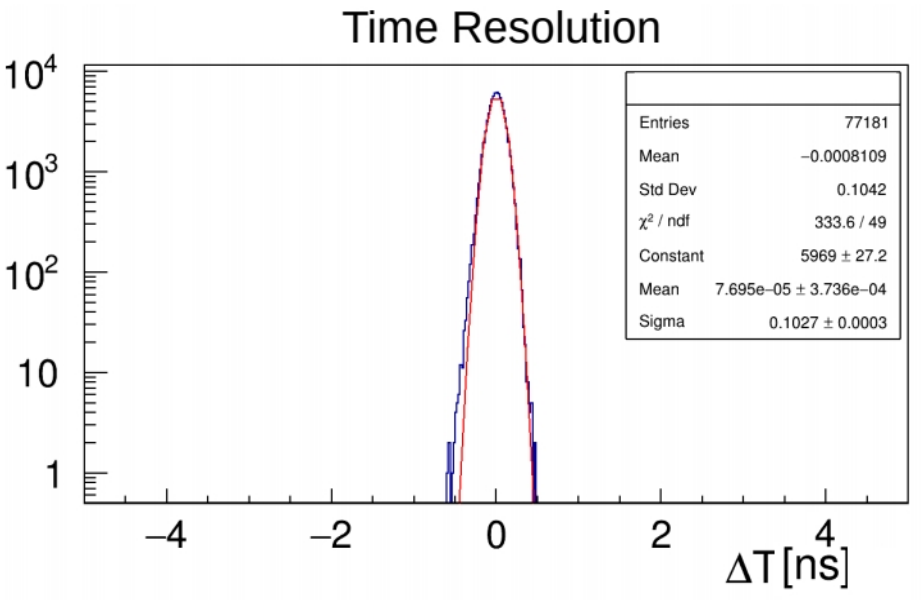

Figure 23: Time resolution from run 160.

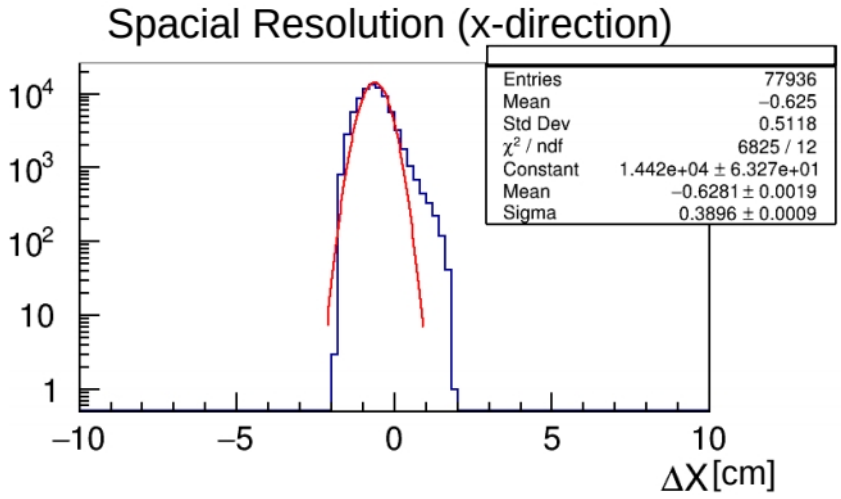

Figure 24: Spacial resolution in x-direction from run 160.

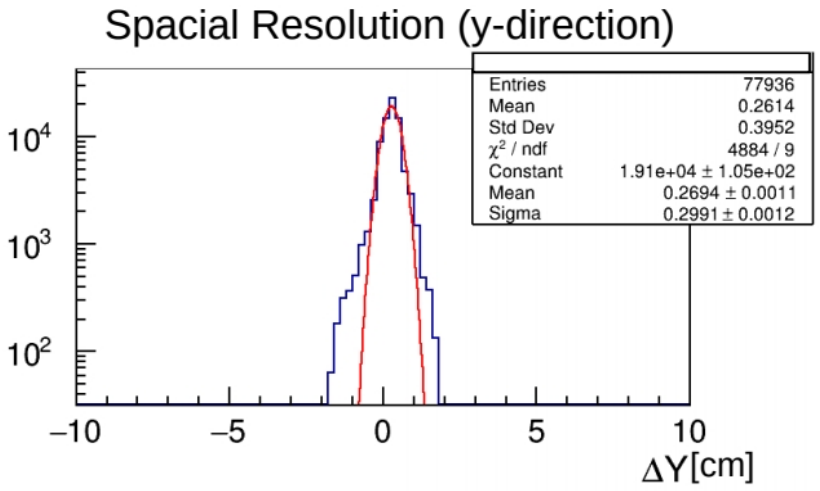

Figure 25: Spacial resolution in y-direction from run 160.

5 Summary and Outlook

The performance of a detector prototype built at CERN was tested at the mCBM setup during the March 2019 beamtime to evaluate a new thin low resistive float glass. This glass is used for the resistive plates in the MRPC and is said to have a resistivity of $3.8{\cdot}10^{10}\Omega cm$ with a thickness of only 0.4mm. To test the performance a high voltage scan was done with a maximum efficiency of 44% at ±9.4kV at an average rate of $7.9{\cdot}10^{9}$Hz. The high voltage scan with over 50% efficiency less than expected also showed a saturation of efficiency which is unexpected at such low efficiencies. In order to investigate if the detector was sufficiently efficient but the read out chain lost data a rate scan was also analyzed. Here one could see a clear dependence of the efficiency and the rate with a maximum efficiency of 59.1% at ±9.3kV at an average rate of $5.6 \cdot 10^{3}$Hz. However, the runs where the thick target was used showed better efficiencies than the runs with a thin target. This effect can at least partly be explained by the extrapolating tracking setup and the delta electrons which were present in high numbers during this mCBM beamtime. Also, the relationship between the rate measured by the detector was compared to the currents measured in the detector. Here a trend was visible that at high rates the rate measured by the detector does not follow the currents linearly anymore. However, a clear conclusion could not be made since the errors on the measurement were too large especially for high rates. The resolution was measured to be (102.7 ± 0.3)ps for the time, (3.896 ± 0.009)mm for the spacial resolution in x-direction and (2.991 ± 0.012)mm for the spacial resolution in y-direction. Based on the measurements made so far it is not possible to judge how well the detector or the glass performed. After the beamtime at mCBM the detector was brought back to Heidelberg to continue the detector tests with cosmic muons. In Heidelberg the detector showed an efficiency up to 70% and a time resolution of about 80ps.

Looking forward, there are still many open questions that need to be answered. The CBM-TOF group has ordered samples of the new glass to measure the resistivity and to build their own prototypes. A direct comparison to the soda lime glass currently used is needed to figure out how well the new thin low resistive works. In order to do this, two new prototypes will be built in Bucharest by the CBM-TOF group. One will be built with the new glass and one with the soda lime glass in order to have a direct comparison between the two. They will be included in the next mCBM beamtime. The cosmic muon stand in Heidelberg will continue to take data to better

understand the detectors as well as the readout chain. In order to get rid of the delta electrons during the following beamtimes a thick aluminium plate will be part of the mCBM setup right behind the target to shield off the delta electrons from the detectors. As for the analysis it will be important to compare the current and rate measurements from all the mTOF modules and the prototypes because rate dependent data loss was also observed there. It is also planned to upgrade the read out chain by 2021 and change from GBTX, AFCK and FLIB boards to a CRI board.

References

[1] Bengt Friman, Claudia Höhne, Jörn Knoll, Stefan Leupold, Jorgen Randrup, Ralf Rapp and Peter Senger. *"The CBM Physics Book: Compressed Baryonic Matter in Laboratory Experiments"*. Springer Verlag, März 2011.

[2] *Fair baseline technical report*. 2006. `http://inspirehep.net/record/1621651/files/FAIR_BTR_1.pdf`

[3] D. Sauter. *"MRPC Prototype 3a & 3b performance studies at the cosmic radiation test setup of the CBM-TOF group in Heidelberg"*. December 2018.

[4] N. Herrmann. *"Technical Design Report for the CBM Time-of-Flight System (TOF)"*. October 2014.

[5] Christoph Blume. *"Strangeness in Heavy-Ion Collisions"*. September 2015.

[6] E.L.Bratkovskaya, P.Moreau, A.Palmese, W.Cassing, E.Seifert and T.Steinert. *"Signatures of chiral symmetry restoration and its survival throughout the hadronic phase interactions"*. February 2018.

[7] J. Stachel, K. Reygers. *"Lecture: Quark Gluon Plasma Physics"*. April 2019.

[8] Christian Lippmann. *"Particle identification"*. June 2011.

[9] Facility for Antiproton and Ion Research/CBM `https://fair-center.eu/for-users/experiments/cbm-and-hades/cbm.html`

[10] Christian Sturm. *"11th mCBM meeting"*. June 2019.

[11] Z.Liu, M.C.S.Williams, A.Zichichi and R.Zuyeuski. *"A Multigap Resistive Plate Chamber built with thin low-resistive glass:High rate capability with excellent time resolution"*. June 2019.

[12] Z.Liu, F.Carnesecchi, M.C.S.Williams, A.Zichichi and R.Zuyeuski. *"Timing performance study of Multigap Resistive Plate Chamber with different gap size"*. May 2019.

[13] Anna Senger. *"FLUKA simulation: delta electrons in mCBM"*. June 2019.

[14] The CBM colaboration. *"mCBM@SIS18: A CBM full system test-setup for high-rate nucleus-nucleus collisions at GSI / FAIR"*. June 2017. `http://p31769.typo3server.info/fileadmin/fair/experiments/CBM/documents/mcbm-proposal2GPAC-WebVersion0619-SVN7729.pdf`

[15] M. Ciobanu, N. Herrmann, K. D. Hildenbrand, M. Kiš, A. Schüttauf, H. Flemming, H. Deppe, S. Löchner, J. Frühauf, I. Deppner, P. A. Loizeau, and M. Träger. *"PADI, an Ultrafast Preamplifier - Discriminator ASIC for Time-of-Flight Measurements"*. April 2014.

[16] Ingo Deppner. *"Alternative TOF readout"*. April 2019.

[17] Ingo Deppner. *"Development of a fully differential Multi-gap Resistive Plate Chamber for the CBM Experiment"*. November 2013.

[18] J. Rafelski and R. Hagedorn. *"From Hadron Gas To Quark Matter. 1"*. September 1980.

[19] J. Rafelski and R. Hagedorn. *"From Hadron Gas To Quark Matter. 2"*. October 1980.

Ich versichere, dass ich diese Arbeit selbstständig verfasst und keine anderen als die angegebenen Quellen und Hilfsmittel benutzt habe.

Heidelberg, den 18.07.2019

.....
(Nils Heyer)